JOURNAL OF SOLID STATE CHEMISTRY 110, 142–149 (1994)

A New "123" Family: $LnBa_2Fe_3O_z$

III. Ln = Gd

E. García-González,*,[1] M. Parras,* J. M. González-Calbet,*,†[2] and M. Vallet-Regí†,‡

*Departamento de Química Inorgánica, Facultad de Químicas, Universidad Complutense, 28040-Madrid, Spain; †Instituto de Magnetismo Aplicado, RENFE-UCM, Apdo. Correos 155, 28230-Las Rozas (Madrid), Spain; and ‡Departamento de Química Inorgánica y Bioinorgánica, Facultad de Farmacia, Universidad Complutense, 28040-Madrid, Spain

Received February 17, 1993; in revised form August 10, 1993; accepted August 11, 1993

An electron diffraction and microscopy study performed on the system $LnBa_2Fe_3Oz$ has shown the presence of new perovskite-related superstructures as a function of both Ln and oxygen stoichiometry. These materials constitute the members n = 1 (Ln = Dy, Ho), n = 3/2 (Ln = Gd), n = 4/3 (Ln = Gd, when overheated at 1300°C for 15 days), and n = 2 (Ln = Nd) of a homologous series with the general formula $Ln_{1/3}Ba_{2/3}FeO_{3-(1/2n+1)}$. A modulated structural approach to $LnBa_2Fe_3O_z$ over the description of these phases is discussed.

INTRODUCTION

We have reported in previous papers (1, 2) a study of the accommodation of compositional variations in $Ln_{1/3}Ba_{2/3}FeO_{3-y}$ (Ln = Nd, Sm, Eu, Dy, and Ho) perovskite-related materials, on which diverse structural arrangements occur due to the different distribution of anionic vacancies associated with the lanthanide element introduced in the A positions of the perovskite sublattice.

Taking into account the results obtained in the microstructural characterization of these materials, the formation of two different members of the $Ln_{1/3}Ba_{2/3}FeO_{3-(1/2n+1)}$ family has been described. The n = 1 term is constituted by $Dy(Ho)_{1/3}Ba_{2/3}FeO_{2.67}$ and the n = 2 term is the $Ln_{1/3}Ba_{2/3}FeO_{2.80}$ phase. Two structural models based on the ability of iron to adopt square-pyramidal and octahedral coordination when barium is occupying the A position on the perovskite-type ABO_3 compounds (3–5) were proposed. The n = 1 member, also reported by Huang *et al.* in the structural determination of $YBa_2Fe_3O_8$ (6, 7), has a tetragonal symmetry lattice with parameters $a_c \times a_c \times 3a_c$ ($P4/mmm$ as possible space group) and can be described as an alternating stacking sequence of two square pyramids and one octahedron along the c axis. The n = 2 term also corresponds to a tetragonal symmetry unit cell with parameters $a_c \times a_c \times 5a_c$, described as the ordered alternation of three octahedra and two square pyramids along the c axis following the stacking sequence ...|OPOPO|OPOPO|... (O is octahedron, P is square pyramid).

Oxygen stoichiometries between these two values are achieved when the lanthanide is samarium or europium, and a short-range order situation takes place. These materials exhibit the characteristics of an incommensurately modulated structure, the wave vector q varying continuously with anionic composition. The structure becomes commensurate (superstructure) for some fixed quantities of anionic vacancies (q = 1/3 a^* in $O_{2.67}$ and q = 2/5 a^* in $O_{2.80}$).

On the materials under study, the anionic composition was related to the lanthanide element at some fixed synthesis conditions. If the experimental conditions are varied, diverse anionic stoichiometries can be obtained for the same lanthanide introduced, which would correspond to other terms of the $Ln_{1/3}Ba_{2/3}FeO_{3-(1/2n+1)}$ family. In this way, we have prepared two different oxygen compositions of the $Gd_{1/3}Ba_{2/3}FeO_{3-y}$ material by changing the thermal treatment in the synthesis procedure. The y values obtained do not correspond to any integer n value of this family but are intermediate between the n = 1 and n = 2 terms mentioned above.

The microstructural characterization by means of selected area electron diffraction (SAED) and high resolution electron microscopy (HREM) has enabled us to go deeper inside into the crystal chemical explanation of the "123" family.

[1] Work submitted in part for the fulfillment of the degree of Doctor of Chemistry by E.G.G., Universidad Complutense, Madrid, April 1992.

[2] To whom correspondence should be addressed.

0022-4596/94 $6.00

EXPERIMENTAL

Samples of nominal composition $Gd_{1/3}Ba_{2/3}FeO_{3-y}$ were prepared by heating stoichiometric mixtures of $BaCO_3$, Gd_2O_3, and α-Fe_2O_3 of AnalaR quality at 1300°C for 72 hr in air. The homogeneous black products were quenched to room temperature in the platinum crucibles used for synthesis. Part of the sample was treated at 1300°C for 15 days. In the following, the former material will be called Gd1 and the overheated sample will be referred to as Gd2.

The oxidation state of iron was determined by titration after dilution in 3N HCl with an excess of Mohr salt.

Powder X-ray diffraction was performed on a SIEMENS D-5000 diffractometer with a graphite monochromator and using Cu$K\alpha$ radiation.

Selected area electron diffraction (SAED) was carried out on a JEOL 2000FX electron microscope, fitted with a double tilting goniometer stage (±45°). High resolution electron microscopy (HREM) was performed on a JEOL 4000EX electron microscope fitted with a double tilting goniometer stage (±25°), working at 400 kV. The samples were ultrasonically dispersed in *n*-butanol and transferred to carbon-coated copper grids.

RESULTS AND DISCUSSION

Samples labeled Gd1 and Gd2 were shown by chemical analysis to have the compositions $Gd_{1/3}Ba_{2/3}FeO_{2.74}$ and $Gd_{1/3}Ba_{2/3}FeO_{2.70}$, respectively, which implies a high amount of oxygen deficiency related to the ABO_3 stoichiometry.

The X-ray powder diffraction patterns showed only reflections corresponding to a pseudocubic perovskite-type unit cell. However, the electron microscopy study indicated that these samples were more complex.

Most of the crystals corresponding to the Gd1 sample presented the SAED patterns along the $[001]_c$, $[0\bar{1}1]_c$, and $[\bar{1}11]_c$[3] zone axes shown in Figs. 1a, 1b, and 1c, respectively. All the diffraction maxima can be indexed on the basis of a cubic perovskite cell. By tilting around b^*, the $[010]_c$ and $[\bar{1}10]_c$ reciprocal lattice projections (Figs. 2a and 2b) are obtained, showing an eightfold superstructure along the c^* axis. The HREM images along these zone axes (Figs. 3a and 3b, respectively) show ordered fringes with a d-spacing of 3.12 nm ($\simeq 8a_c$).

The reciprocal lattice deduced from the electron diffraction patterns corresponds to a tetragonal symmetry real cell of parameters $a_c \times a_c \times 8a_c$ with $P4/mmm$ as possible space group.

When the Fe (IV) amount decreases, i.e., in the Gd2 sample, significant differences appear. Most of the crystals showed the same structural features. Although the SAED patterns along the $[001]_c$, $[0\bar{1}1]_c$, and $[\bar{1}11]_c$ zone axes are analogous to those observed for the Gd1 sample, an 11-fold superstructure can be seen along the c^* direction. Figures 4a and 4b show the SAED patterns of the Gd2 material along the [010] and $[\bar{1}10]$ zone axes.

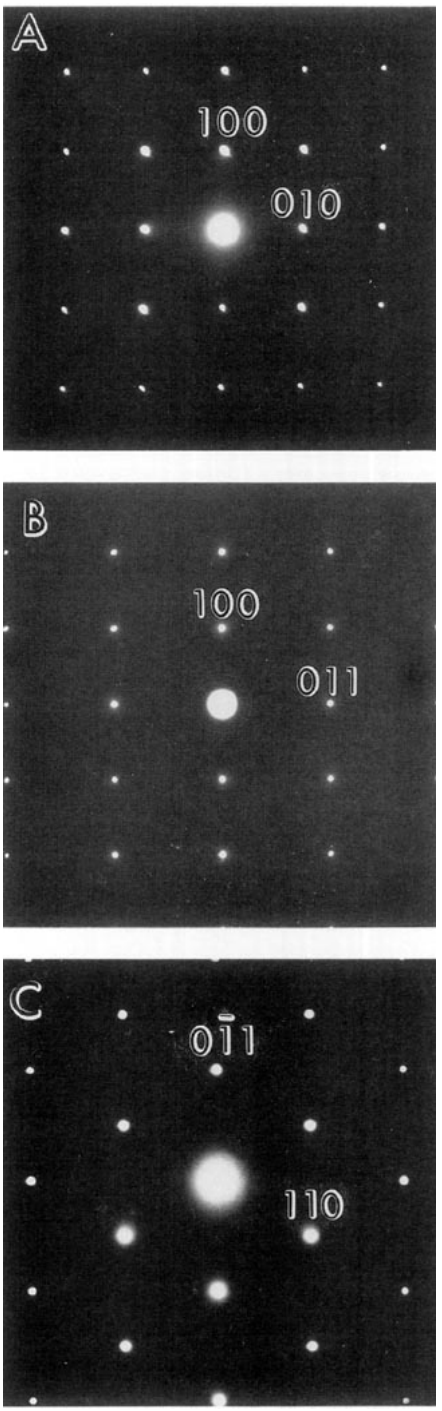

FIG. 1. Electron diffraction patterns corresponding to the $Gd_{1/3}Ba_{2/3}FeO_{2.75}$ sample along (a) $[001]_c$, (b) $[0\bar{1}1]_c$, and (c) $[\bar{1}11]_c$ zone axes.

[3] Subindex c refers to the basic perovskite subcell.

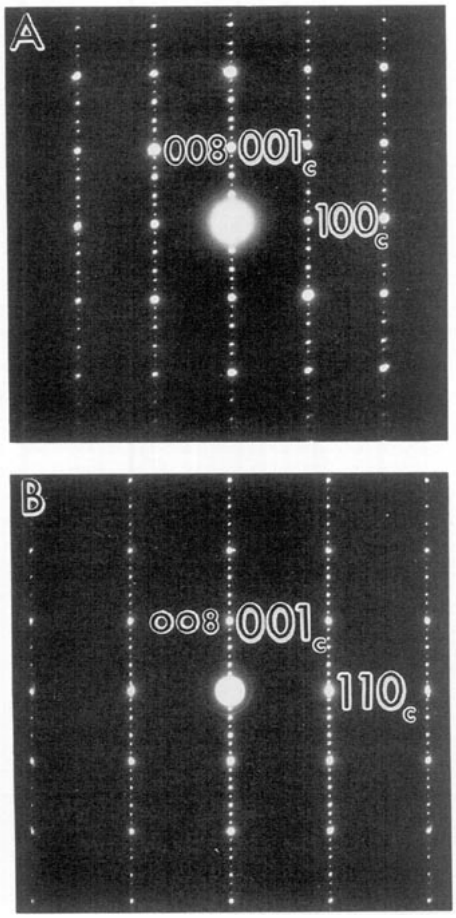

FIG. 2. Electron diffraction patterns for $Gd_{1/3}Ba_{2/3}FeO_{2.75}$ along the (a) $[010]_c$, and (b) $[\bar{1}10]_c$ zone axes.

The corresponding HREM images (Figs. 5a and 5b, respectively) reveal the presence of lattice fringes at 4.3 nm ($\simeq 11a_c$) along the $[001]_c$ direction in a well ordered material.

Again, the results obtained by electron diffraction lead to a tetragonal symmetry real space cell with parameters $a_c \times a_c \times 11a_c$ and $P4/mmm$ as possible space group.

However, it is worth recalling that in both samples, a small fraction of crystals showed a different situation. This kind of crystal, previously described in Ref. (2) (see Fig. 5 in Ref. (2)), shows a short-range order situation, probably due to a lower oxygen content. This could account for the slight differences between theoretical and experimental compositions.

From the above results, it is clear that across the anionic composition range in the $Ln_{1/3}Ba_{2/3}FeO_{3-(1/2n+1)}$ family, several superstructures along the c direction take place, their magnitude varying as a function of oxygen composition.

TABLE 1
Experimental and Theoretical Anionic Composition for Every Superstructure

Experimental composition	Theoretical oxygen content per unit formula	Subcell multiplicity
$Nd_{1/3}Ba_{2/3}FeO_{2.80}$	$O_{2.80}$	$a_c \times a_c \times 5a_c$
$Gd_{1/3}Ba_{2/3}FeO_{2.74}$	$O_{2.75}$	$a_c \times a_c \times 8a_c$
$Gd_{1/3}Ba_{2/3}FeO_{2.70}$	$O_{2.727}$	$a_c \times a_c \times 11a_c$
$Dy(Ho)_{1/3}Ba_{2/3}FeO_{2.67}$	$O_{2.677}$	$a_c \times a_c \times 3a_c$

Taking into account the oxygen content obtained by chemical analysis and the possibility of iron adopting five- and sixfold coordination, some structure models based on the alternation of square-pyramidal and octahedral polyhedra have been proposed for each composition.

Thus, for the $Gd_{1/3}Ba_{2/3}FeO_{2.74}$ material, a unit cell constituted by four octahedra and four square pyramids would give the best agreement with the anionic stoichiometry (see Table 1). The relative arrangement of the polyhedra along the c direction giving rise to an eightfold superstructure could fit, according to the contrast observed in the corresponding HREM images (Figs. 3a and 3b), to a . . . |OPOPPPOPO|OPOPPPOPO| . . . stacking sequence (Fig. 6a). The lack of reflections at $(\frac{1}{2}\ 0\ 0)^*$ and $(0\ \frac{1}{2}\ 0)^*$ suggests that the oxygen vacancies are randomly distributed in the corresponding (001) planes.

The interpretation of the image contrast in the HREM images obtained has also been made with the help of a simulation program using the multislice method (8). Image calculations were carried out under the following imaging conditions: sample thickness between 1.0 and 5.5 nm, $\Delta f = -30$ to -70 nm, $C_s = 1.0$ nm, $C_c = 1.7$ nm, beam divergence angle $= 0.8 \times 10^{-3}$ rad, and accelerating voltage = 400 kV.

The agreement is satisfactory for the following conditions:

—$[010]_c$ projection: $\Delta f = -70$ nm and sample thickness of 4.0 nm;

—$[\bar{1}10]_c$ projection: $\Delta f = -60$ nm and sample thickness of 4.5 nm.

Both images are inset on Figs. 3a and 3b, respectively.

For the $Gd_{1/3}Ba_{2/3}FeO_{2.70}$ material, and considering the structural models previously proposed, the sequence of polyhedra that would lead to an apparent 11-fold superstructure along the c direction would be constituted by five octahedra and six square-pyramids, of which the theoretical anionic composition per unit formula is $O_{2.727}$. According to the contrast observed in the high resolution micrographs (Figs. 5a and 5b), the stacking sequence . . . |OPOPPPOPPOPO|OPOPPPOPPOPO| . . . can be proposed (Fig. 6b). As in the first case, the structural

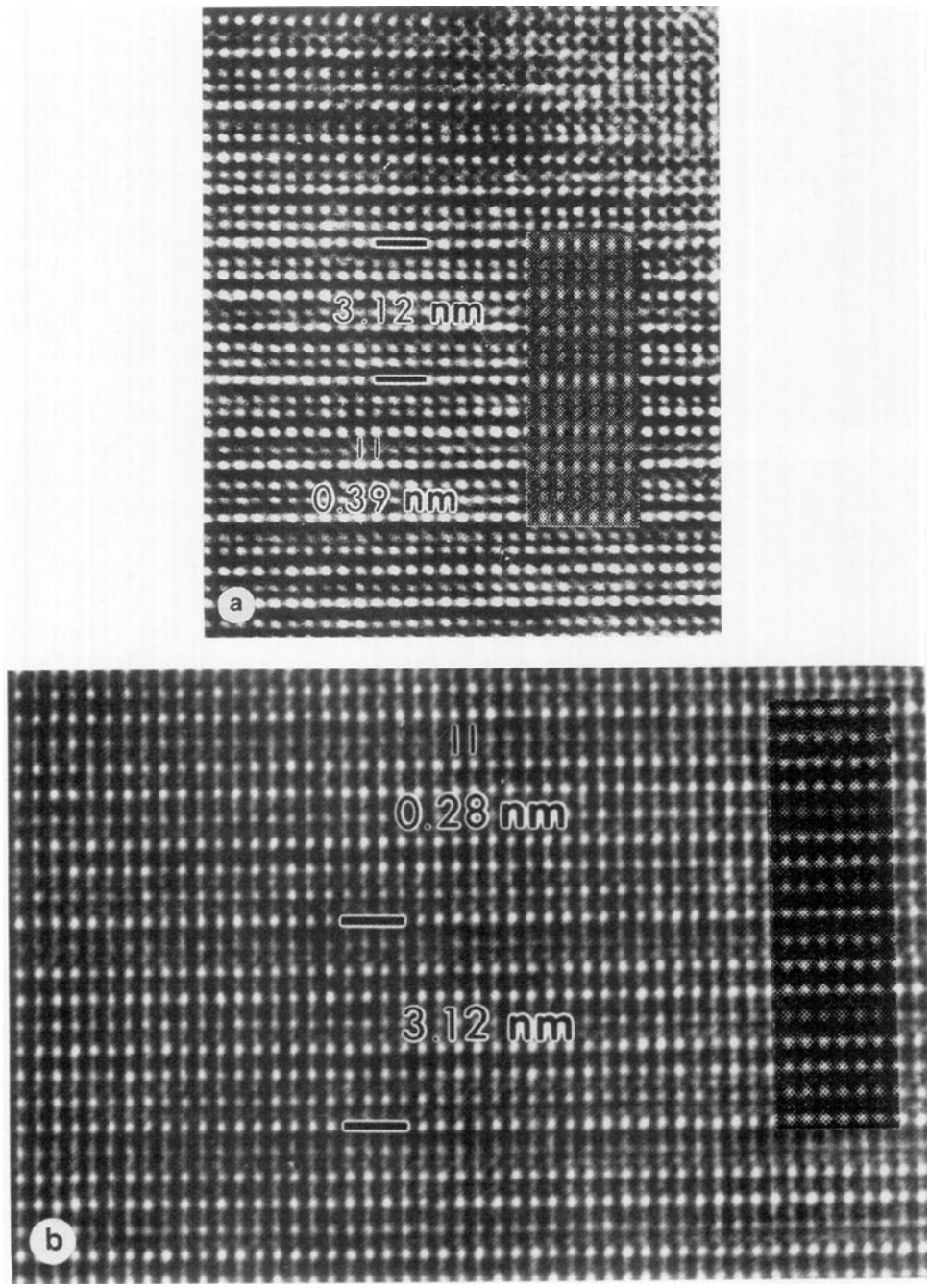

FIG. 3. High resolution images for the $Gd_{1/3}Ba_{2/3}FeO_{2.75}$ material along the (a) $[010]_c$ and (b) $[\bar{1}10]_c$ zone axes. In both images black dots correspond to *Ln*, Ba, and Fe atoms. The corresponding calculated images (close to Scherzer focus conditions: see text) are inset.

model proposed considers disorder of the anionic vacancies, due to the lack of reflections at $(\frac{1}{2}\ 0\ 0)^*$ and $(0\ \frac{1}{2}\ 0)^*$ and equivalent positions.

Image calculation was developed under the same conditions previously reported, the best fit between experimental and calculated images being obtained for the following values of defocus and crystal thickness:

$[010]_c$ projection: $\Delta f = -70$ nm and sample thickness of 4.0 nm;

$[\bar{1}10]_c$ projection: $\Delta f = -60$ nm and sample thickness of 4.0 nm.

According to both, the oxygen content and the contrast observed in the corresponding HREM images, the only possible models for both materials, are those presented

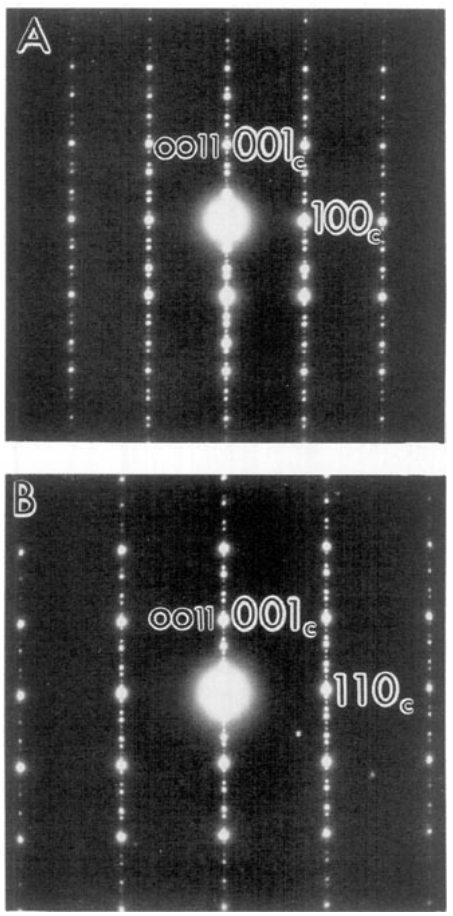

FIG. 4. Electron diffraction patterns for $Gd_{1/3}Ba_{2/3}FeO_{2.727}$ along the (a) $[010]_c$, and (b) $[\bar{1}10]_c$ zone axes.

in Figs. 6a and 6b. Different O : P ratios or arrangements, as well as the introduction of tetrahedra in the proposed models, would not agree with the experimental results presented.

All these results suggest that a series of superstructures of the perovskite-type ABO_3 structure (9) occurs across the composition range between $ABO_{2.67}$ and $ABO_{2.80}$, the decrease of the oxygen content with respect to the ABO_3 stoichiometry being accommodated by distortion of the anion array and generating new coordination polyhedra (square pyramids). Those superstructures appear only for well defined anionic composition values, as shown in Table 1.

These phases can be considered components of a series of general formula $Ln_{1/3}Ba_{2/3}FeO_{3-(1/2n+1)}$ in which they are the members corresponding to $n = 1, \frac{4}{3}, \frac{3}{2}$, and 2, respectively.

As previously stated (2), intermediate compositions cannot be constructed of ordered (or partially ordered) units of neighboring simple superstructures.

Taking into account the above considerations, and in order to explain in a systematic way the structural aspects of this family of compounds, it is useful to describe them by using a modulated structure approach.

The set of reflections always appearing along the c^* direction can be divided in all cases into two different groups:

—stronger intensity maxima G corresponding to an average metrically simple cubic structure, and

—a weaker set of satellite reflections at $G \pm mq$.

Figure 7 shows a schematic illustration of the appearance of the (001) diffraction pattern rows for the $Ln_{1/3}Ba_{2/3}FeO_{3-y}$ compounds.

The wave vector q varies continuously with anionic composition, and takes the exact values $q = \frac{2}{5}, \frac{3}{8}, \frac{4}{11}$, and $\frac{1}{3}$ for $3 - y = 2.80$, 2.75, 2.727, and 2.677, respectively. In these cases, the modulation has become a superlattice, the satellite reflections turning into superlattice reflections. The relationship between the q values stoichiometries is such that $y = 1 - 2q$, provided that $q = n/(2n + 1)$. Thus, the general formula $Ln_{1/3}Ba_{2/3}FeO_{3-(1/2n+1)}$ becomes $Ln_{1/3}Ba_{2/3}FeO_{3-(1/2-q)}$.

Our first studies in this direction showed the appearance of incommensurate satellite reflections at $\simeq \frac{2}{5}a^*$ for the $Sm_{1/3}Ba_{2/3}FeO_{2.78}$ and $Eu_{1/3}Ba_{2/3}FeO_{2.76}$ materials; the high resolution images on Fig. 5 of Ref. (2) showed contrast variations along a that corresponded to double and triple the perovskite subcell. The 1 : 1 ratio of both types of spacing in the crystal would lead to satellite reflections at exactly $\frac{2}{5}a^*$, their ordered distribution giving rise to fivefold superstructure reflections, as observed in $Nd_{1/3}Ba_{2/3}FeO_{2.80}$. Figures 3a and 3b can be interpreted following the same argument; the observed contrast variations correspond to triple, double, and triple perovskite-type blocks arranged in an ordered way along the c axis in the unit cell. The q value is exactly $\frac{3}{8}a^*$.

For the $3 - (1 - 2q) = 2.727$ anionic composition, an ordered distribution of triple and double perovskite-type blocks in a 3 : 1 ratio (Figs. 5a and 5b) leads to $q = \frac{4}{11}a^*$.

It is possible to predict the structures of other n values, by simply varying the double to triple perovskite-type blocks contrast ratio:

—triple : double : : 4 : 1 would lead to $q = \frac{5}{14}a^*$ (member $n = \frac{5}{4}$ in the series), where the alternation of six octahedra and eight square pyramids along the c axis would give an anionic composition $O_{2.71}$;

—triple : double : : 5 : 1 would lead to $q = \frac{6}{17}a^*$ (member $n = \frac{6}{5}$ in the series), where the alternation of seven octahedra and 10 square pyramids along the c axis would give an anionic composition $O_{2.706}$.

Continuing in this way, the magnitude of the modulation wave-vector is $\frac{1}{3}a^*$ for the $3 - (1 - 2q) = 2.67$ composition, which corresponds to triple the perovskite subcell (see Fig. 3 in Ref. (1)).

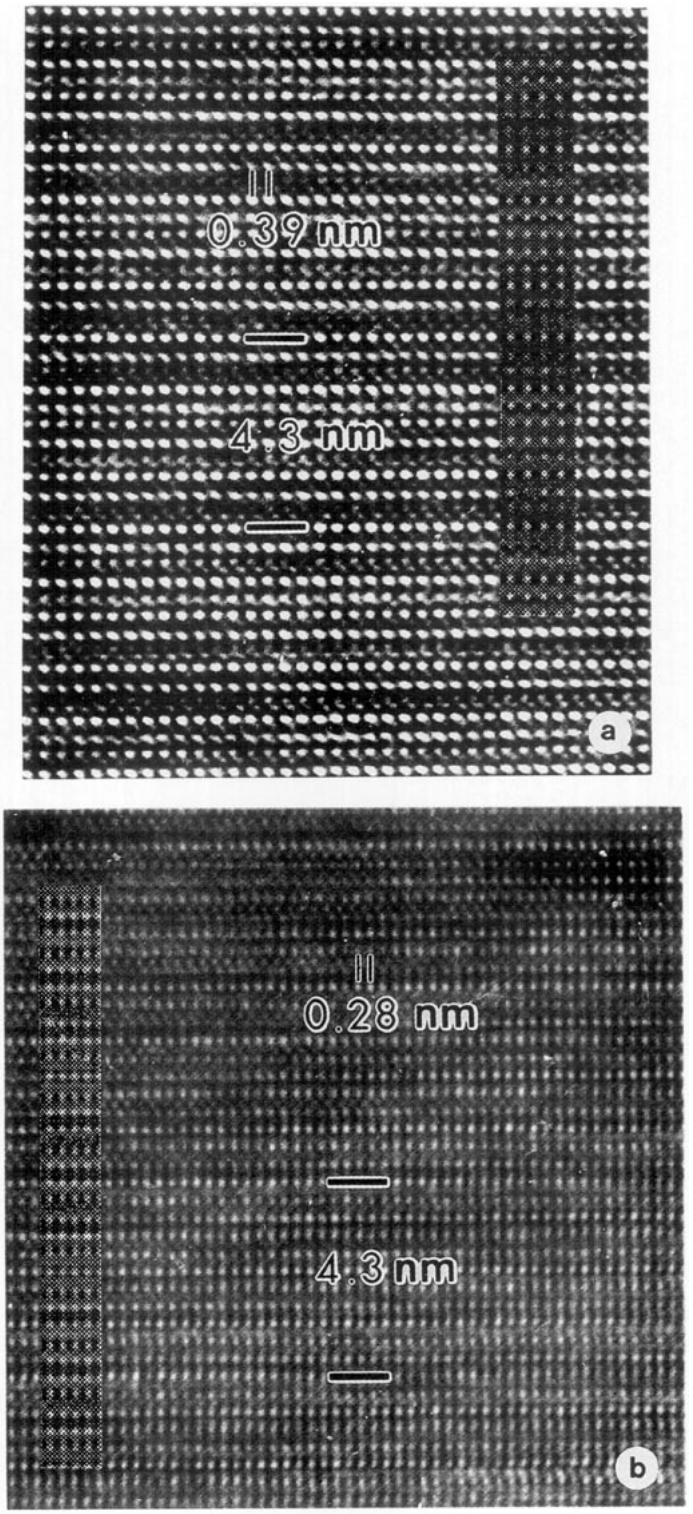

FIG. 5. High resolution images for the $Gd_{1/3}Ba_{2/3}FeO_{2.727}$ material along the (a) $[010]_c$, and (b) $[\bar{1}10]_c$ zone axes. In both images black dots correspond to *Ln*, Ba, and Fe atoms. The corresponding calculated images (close to Scherzer focus conditions: see text) are inset.

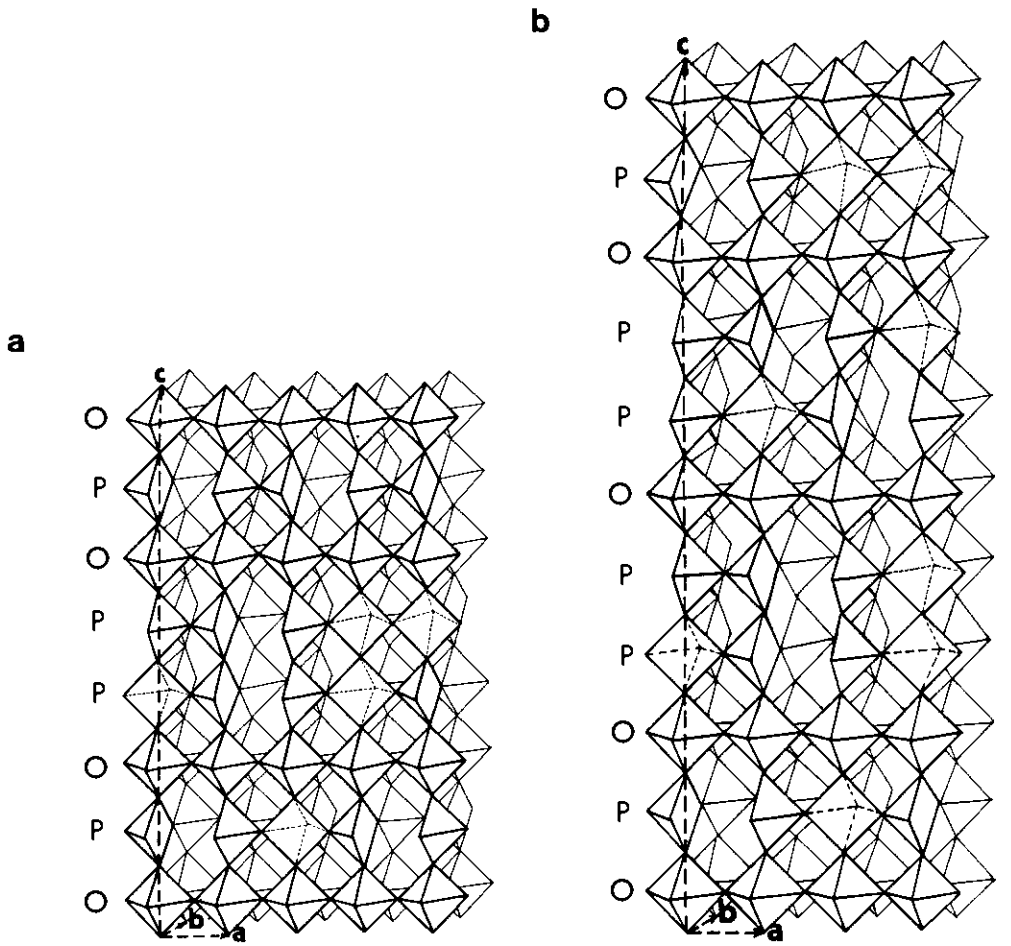

FIG. 6. (a) Structural model proposed for $Gd_{1/3}Ba_{2/3}FeO_{2.75}$; (b) Structural model proposed for $Gd_{1/3}Ba_{2/3}FeO_{2.727}$.

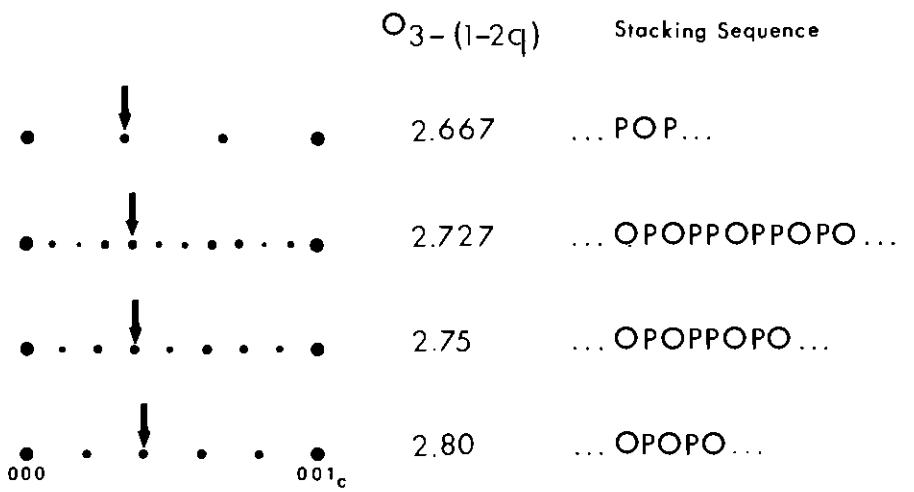

FIG. 7. Schematic illustration of the (001) diffraction pattern rows for $Ln_{1/3}Ba_{2/3}FeO_{3-(1-2q)}$ phases. Arrows indicate the positions of the first-order satellite reflections.

Thus, a modulated structure approach to $Ln_{1/3}Ba_{2/3}FeO_{3-y}$ presents an advantage over the description of these phases as different members of a homologous series of compounds; the description of the diffraction maxima as corresponding to $G \pm mq$ can be applied when a superstructure approximation is valid (for the values $q = \frac{2}{5}, \frac{3}{8}, \frac{4}{11}$, and $\frac{1}{3}$) and for intermediate anionic compositions, and constitutes a systematic way of studying the crystal structure across the composition range.

ACKNOWLEDGMENTS

We acknowledge the financial support of C.I.C.Y.T. (Spain) through research projects MAT 90-0858-CO2-02 and MAT 91-0331, and the MIDAS program. E.G.G. also thanks the Spanish Ministry of Education for a supporting grant. We are also grateful to Mr. A. Garcia for valuable technical assistance and to Dr. A. Landa for helpful discussions during the present work.

REFERENCES

1. E. García-González, M. Parras, J. M. González-Calbet, and M. Vallet-Regí, *J. Solid State Chem.* **104,** 232 (1993).
2. E. García-González, M. Parras, J. M. González-Calbet, and M. Vallet-Regí, *J. Solid State Chem.* **105,** 363 (1993).
3. J. C. Gibb and M. Matsuo, *J. Solid State Chem.* **81,** 83 (1989).
4. M. Parras, L. Fournes, J. C. Grenier, M. Pouchard, M. Vallet, J. M. González-Calbet, and P. Hagenmüller, *J. Solid State Chem.* **88,** 261 (1990).
5. X. Zou, S. Hovmöller, M. Parras, J. M. González-Calbet, M. Vallet-Regí, and J. C. Grenier, *Acta Crystallogr. Sect. A* **49,** 27 (1993).
6. Q. Huang, P. Karen, V. L. Karen, A. Kjekshus, J. W. Lynn, A. D. Mighell, N. Rosov, and A. Santoro, *Phys. Rev. B Condens. Matter.* **45,** 9611 (1992).
7. P. Karen, P. H. Andresen, and A. Kjekshus, *J. Solid State Chem.* **101,** 48 (1992).
8. NCEMSS Programm, National Center for Electron Microscopy, Materials and Chemical Sciences Division, Lawrence Berkeley Laboratory, University of California, Berkeley, California, 1989.
9. H. D. Megaw, *Proc. Phys. Soc.* **58(2),** 133 (1946).